www.czasopisma.pan.pl PAN www.journals.pan.pl

ARCHIVES of FOUNDRY ENGINEERING

ISSN (2299-2944)
Volume 2025
Issue 1/2025

150 – 158

18/1

10.24425/afe.2025.153785

Published quarterly as the organ of the Foundry Commission of the Polish Academy of Sciences

Examination of the Effect of Chemical Composition on Laser Polished Cast Irons with Spheroidal Graphite

O. Özaydin [a, *], L. Kreinest [b], J. Schüssler [a], E. Willenborg [b], A. Bührig-Polaczek [a]

[a] Foundry Institute of RWTH Aachen, Germany

[b] Fraunhofer Institute for Laser Technology, Germany

* Corresponding author: E-mail address: o.oezaydin@gi.rwth-aachen.de

Received 30.07.2024; accepted in revised form 09.01.2025; available online 26.03.2025

Abstract

Spherical Graphite Cast Iron (SGI) alloys have been used as a material in mold making for deep-drawing dies and glass molds due to their excellent machinability and thermal conductivity. Moreover, other advantages of SGI alloys are their supreme castability, to cast complex geometries in comparison to steel, and the use of up to 90 % recycled materials, especially steel scrap. This leads to a significant reduction of material and energy usage, thereby contributing to both financial savings and ecological benefits. Nevertheless, the mold application of SGI alloys is restricted by inherent limitations, including low hardness values and high surface roughness after machining and even after manual polishing. To overcome these drawbacks a laser polishing process can be beneficial to obtain a graphite-free and steel-like hard surface and to enable a very low surface roughness, optionally in combination with a final manual polishing step. According to the state of the art, the graphite in the SGI structure could not yet be entirely removed from the surface layer by laser polishing, which on one hand leads to a higher roughness and on the other hand raises the risk of cracks. In the current investigations, the SGI alloys with different chemical compositions were cast in three different geometries, machined and subsequently laser polished. After laser polishing, remelting depth and the tendency for surface cracks were investigated. In addition, the influence of graphite morphology on the laser polishing process was examined for these three alloys and three different geometries (wall thicknesses), which all have influences on the microstructure formation. This led to laser polishing parameters to produce a graphite-free, steel-like surface on SGI.

Keywords: Cast iron with spheroidal Graphite (SGI), Casting defects, Graphite, Laser polishing, Microstructure

1. Introduction

Today, hot-work steels are widely used as mold materials due to their excellent mechanical properties and high corrosion resistance at operating temperatures. However, in the last decades, increasing costs and environmental concerns have encouraged researchers to work on alternatives. Cast iron can be a good alternative due to its low costs and its suitability for recycling materials such as steel scrap. The excellent properties and castability of ductile cast iron have led to an increasing use of this material for critical engineering applications in recent years [1-3]. Spheroidal graphite cast irons (SGI) in particularly are distinguished from other options by their good machinability and high thermal conductivity (e.g. ≈36W/K/m for EN-GJS-400-15 compared to ≈25 W/K/m for 1.2343). But low wear resistance due to low hardness and high roughness values prevent this alternative material from being widely used as a mold material. In this study, a laser polishing process that can minimize these disadvantages is investigated. The main idea is based on the fact that after laser

polishing the surface layer is hardened and thus has better wear resistance and that laser polishing can produce a defect-free surface layer enabling a high gloss finish e.g., by a subsequent mechanical polishing step after laser polishing. Undoubtedly, the results of the applied laser polishing process can be influenced by many different parameters. One of the most important of these parameters is the variation in the chemical composition of the material being laser polished. In this study, laser polishing of cast iron samples with three different Si levels and their effects on the surface were investigated. Ductile cast iron can be categorized into three different types according to its matrix: ductile cast iron with ferritic matrix, ductile cast iron with pearlitic matrix and ductile cast iron with ferrite-pearlitic matrix. The ferritic matrix has superior ductility and machinability [2]. Therefore, in this study a ferritic matrix material was chosen.

To create different grades of iron, additional alloying elements are also present and under control.

Alhussein et al. worked on the influence of silicon and additional elements on the mechanical behaviour of ferritic ductile cast iron. The primary aim is to look into how the mechanical characteristics and microstructure of ductile iron are affected by changes in silicon content. Finding the silicon range in iron that permits good properties (strength, ductility, and resilience) is the aim of their study. As a result, the authors concluded that increasing silicon content in ductile iron increased the material tensile strength and decreased its ductility and the impact energy necessary to failure. Varying the silicon content did not affect the ferrite grain size and the silicon was highly segregated around graphite nodules and little along the joints of eutectic cells. This important gradient is the origin of the initiation and propagation of cracks. It is possible to conclude that a high silicon content favourites brittle crack fracture [5].

Nickel, Copper and Molybdenum can be added in small amounts (0.1-1%) to improve mechanical properties. On the other hand, elements such as Cerium, Barium and Aluminum added in very low amounts (0.003-0.1%) can also change the graphite morphology. These additional alloying elements help to increase the number of small spheroid graphite due to the silicon effect, resulting in a refined microstructure. It should be noted that the amount of additional alloying elements is important and that over-limit additives can have negative effects on microstructure and mechanical properties [4,5].

Hatate et al. worked on the influences of graphite shapes on wear characteristics of austempered cast iron. Comparison of flake graphite cast iron (LGI), compacted graphite cast iron (CGI) and spheroidal graphite cast iron (SGI) materials, Y-block molds were used for each material to avoid any variation in cooling rates. Decrease in graphite nodularity results in increased wear loss at the initial wear stage. It is because lower graphite nodularity results in a shorter average matrix distance between graphites and also a larger stress concentration factor at graphite tips [6]. Also, the dynamic impact properties of ferritic cast iron are affected by the quantity of graphite nodules and the nodularity [5].

The process of solidification leads to segregation of silicon. In ductile cast iron these segregations weaken its resistance and cause brittle fractures of the material. Therefore, by increasing the silicon content the material resilience decreases.

Laser polishing of ductile cast iron is based on remelting of a thin surface layer by continuous laser radiation. In the molten state the surface is smoothed by the surface tension. Compared with manual polishing, laser polishing can greatly save time and improve work efficiency. As it is not based on ablation but on remelting, different surface topographies are achieved. But the main difference is that the remelted layer of the cast iron gets homogenized and graphite inclusions that lead to surface defects in mechanical polishing are removed. A laser treated surface of cast iron can be divided into three zones that are called melt zone (MZ), heat affected zone (HAZ) and bulk material zone (BMZ) [7-11]. The martensite strengthening process is accompanied by the generation of retained austenite and it is indicated that for higher retained austenite contents (over 40%), the observed cracking in melt zone was due to an increment in the tensile stresses from the lower specific volume of retained austenite compared to martensite [9,10].

The remelting depth in laser polishing typically range from 20 to 100 µm, but it can also be much larger. Kiedrowski et al. [12] and Ukar et al. explored the laser remelting of EN-GJS-700-2 and were able to reduce the quantity and size of graphite particles in the remelted surface layer. Remelting depths of d = 350 µm were achieved [13-15]. Benyounis et al. also found that the laser remelting of spheroidal cast iron dissolves most of the graphite particles. They obtained a remelted layer with a remelting depth of d = 500 µm which includes retained austenite, martensite and cementite [17]. Pagano et al. [18] also demonstrated that laser remelting results in a reduction of graphite content within the remelting zone, while obtaining a remelted layer containing austenite.

Laser polishing comes in two different process variations: macro and micro polishing. For macro polishing, continuous wave laser radiation is usually utilized. As the laser beam is directed across the surface during macro polishing, a continuous melt pool is produced [19]. Although macro polishing can result in a remelting depth of up to 200 µm, this is typically between 30 and 100 µm [20]. Micro polishing is done by pulsed laser radiation. Every laser pulse creates discrete melt pools, and the material resolidifies before the subsequent laser pulse reaches the surface [19]. Pulsed laser polishing uses less power than continuous wave laser polishing [21]. Features with shorter wavelengths are mainly affected by shorter laser pulse durations. While still successfully smoothing the surface, pulsed laser polishing enables more accurate control of the melting depth and the heat-affected zone [21]. Micro polishing enables the vaporization of micro edges and a remelting depth between 0.5 and 5 µm [22].

2. Experimental Methods

2.1. Casting

In this paper, the effect of silicon on a laser polished surface is investigated. Although there are many studies in literature on the effect of silicon addition on spheroidal cast iron, there is limited information on the effect of silicon on laser polished surfaces. In this study, castings were made at three different levels of silicon

(see table 1). These samples were then pre-machined by milling and then subjected to laser polishing with appropriate parameters. Finally, the surface conditions were investigated.

In addition to the 3 levels of silicon content, 3 different geometries each were casted based on the literature information that different cooling rates will give different microstructure properties. The geometries were prepared according to the relevant standard DIN EN 1563 [16] as shown in Figure 1.

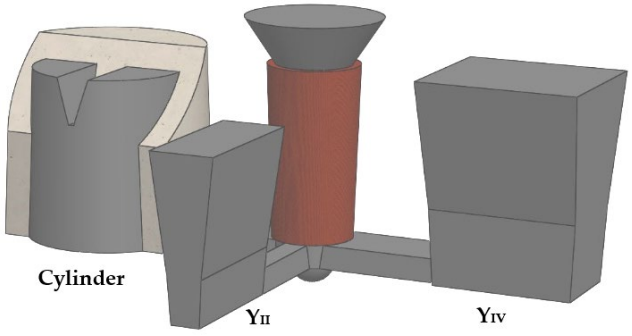

Fig. 1. Schematic representation of the three cast geometries with a gating system [23]

These three different geometries were cast in a sand mold as shown in Figure 2.

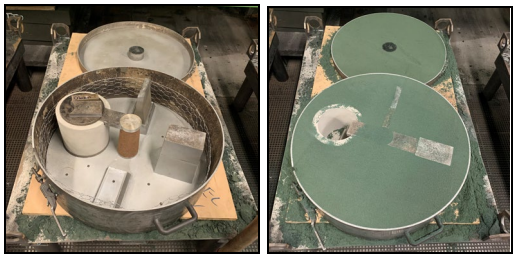

Fig. 2. Sand molds before casting

After the chemical alloy of the material was calculated at the specified levels, the metal was cast by gravity casting after melting and the cast piece shown in Figure 3 was obtained. All samples to be used in the next steps of the study were obtained from these castings.

Fig. 3. Cast Part

In parallel with the information in the literature, the differences in the microstructure of the different geometries can be seen in Figure 4. Since the cylindrical geometry has the lowest cooling rate, it can be easily seen that the graphite in the structure remain larger than in the other samples. Conversely, the casting with Y_{II} geometry has the highest cooling rate and therefore the microstructure with the smallest sized graphite.

Further investigations on the graphite morphology were done as follows: The graphite content is the amount of black and white within a microscope image and calculating the ratio of the black to white surface area. Nodularity refers to the proximity of a graphite particle to a circular shape. Due to the different cooling rates, the geometry with the lowest nodularity and nodule count is the cylinder.

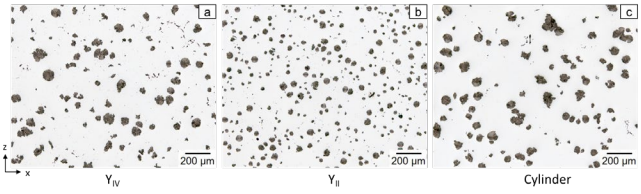

Fig. 4. Light microscopy images of metallographically prepared cross-sections of the three geometries. a: Geometry Y_{IV}. b: Geometry Y_{II}. c: Geometry Cylinder [23]

Table 1.
Chemical Compositions

		C		Si		Mn		P		Cr		Mo		Fe
		wt%	SD	wt%	SD	wt%	SD	wt%	SD	wt%	SD	wt%	SD	wt%
1.	High Si	3,123	0,082	4,251	0,020	0,128	0,001	0,004	0,001	0,066	0,000	0,011	0,002	Bal.
2.	Ave. Si	3,289	0,129	3,522	0,001	0,086	0,001	0,029	0,003	0,060	0,000	0,008	0,001	Bal.
3.	Low Si	3,549	0,020	2,841	0,009	0,113	0,002	0,021	0,002	0,054	0,001	0,009	0,000	Bal.

2.2. Laser Polishing

The laser polishing experiments within this work are carried out with the experimental set-up shown in Fig. 5. The fiber laser used in this system is a redPOWER (SPI Laser Ltd.) emitting cw laser radiation with a wavelength of λ_{em} = 1075 nm - 1080 nm with a maximum laser power of $P_{L,max}$ = 500 W. With a zoom telescope the laser focus diameter can be adapted in the range of

d_L = 120 - 625 µm. The focused laser beam is moved over the workpiece with a galvanometric laser scanner (Scanlab hurrySCAN30). A 5-axis portal machine with NC-control unit positions the work pieces. The process gas chamber can be filled with inert gas to avoid oxidation during laser polishing and an oxygen measurement device measures the residual oxygen content. [23].

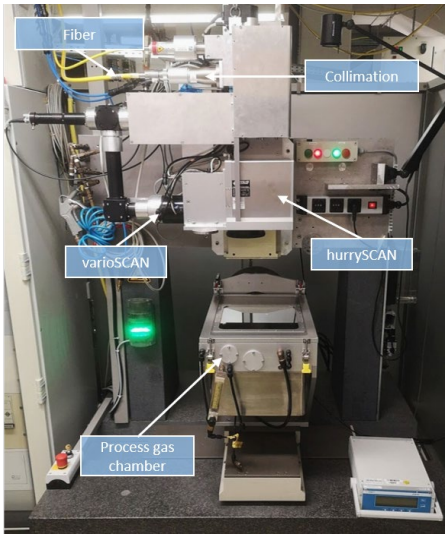

Fig. 5. Experimental set-up for Laser Polishing

Many parameters in the laser polishing process directly affect the resulting surface quality. These parameters include laser power (P_L), number of repetitions (n), scanning velocity (v_{scan}), laser beam diameter (d_L), and track offset (d_y).

Prior to the study shown in this publication an intensive parameter study was carried out to determine suitable parameters for laser polishing of cast iron. It was found that a laser power of P_L=200 W and P_L=300 W and a number of repetitions n = 1, 2 and 4 are appropriate parameters. Thus, combinations of theses parameters were applied to the samples with three different levels of silicon content and the three different geometries. The results are discussed in detail in the "Results and Discussion" section.

2.3. Microstructure Analysis

At the initial stage of microstructural analysis, after the necessary metallographically sample preparations were completed, images were first taken using a light microscope. Graphite content, nodularity, and nodule count values can be calculated using these images. As the size of the graphite spheres is not uniform, statistical methods are used for the evaluation. Several graphite forms can occur within a microstructure as cooling rate, state of nucleation balance and inoculation and alloying elements affect the results.

The analyses of the metallographically prepared cross-sections is done with an Axio Scope A1 light microscope (Carl Zeiss AG, Oberkochen, Germany).

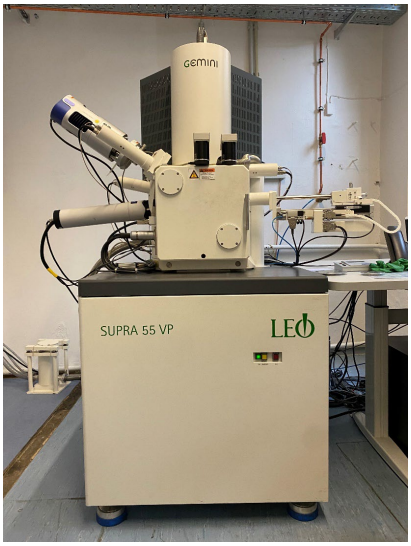

Fig. 6. SEM and EBSD with Supra 55 VP

The analysis of microstructural parameters, especially the graphite phase, is performed using the automated image analysis software AxioVision. For this purpose, electrically conductively embedded and metallographically prepared samples were analyzed in a Zeiss Supra 55 VP scanning electron microscope. Electron backscatter diffraction (EBSD) analyses were performed to investigate the effect of different sensitivity. For this purpose, electrically conductive embedded and metallographically prepared samples are examined under a scanning electron microscope of the Zeiss Supra 55 VP model type (see Fig. 6).

3. Results and Discussion

3.1. Casting Results

The microstructures of the castings with high, average and low Si content (details see Table 1) visualized under the light microscope are shown in Table 2. The three different geometries used in the sand molds (Y_{II}, Y_{IV}, and Cylinder) also result in varying microstructures due to differences in cooling rates.

As shown in Table 2, materials with high, average, and low silicon content can produce differences in castings of the same geometry. These differences are characterized by the calculation of graphite content, nodularity, and nodule count (Fig. 7 to 9).

Before performing these calculations, the expectations were as follows: due to the slow cooling rate in the cylinder part the graphite content should be highest, nodularity should exceed a certain threshold, and the nodule count should be lowest. In this study, these calculations were conducted for the samples with the average silicon content. This approach was chosen because it is anticipated that similar trends will be observed in samples with other silicon levels. This prediction is supported by Table 2, which indicates that differences in geometry have a more pronounced effect than variations in chemical composition. When High-And-Low Si images are analysed for Y_{II} with the same

cooling properties, Si differences do not make a big difference. But for Y_{IV} and Cylinder, differences are seen.

Table 2.
Microstructures

No		Y_{II}	Y_{IV}	Cylinder
		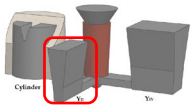	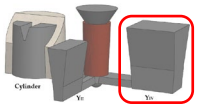	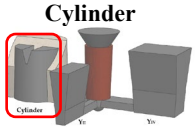
1.	High Si	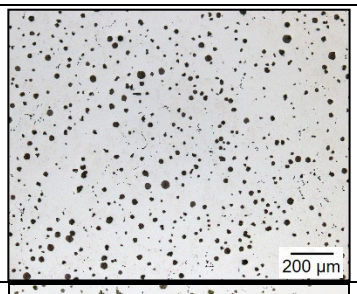	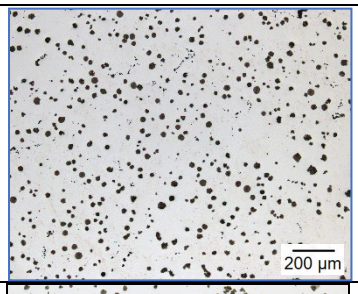	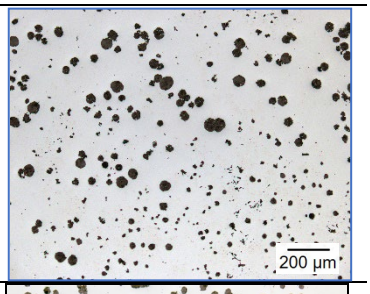
2.	Ave. Si	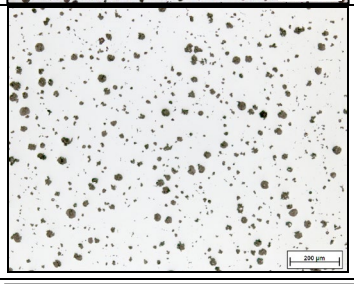	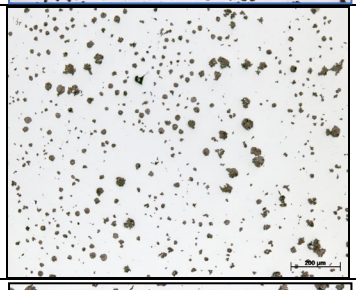	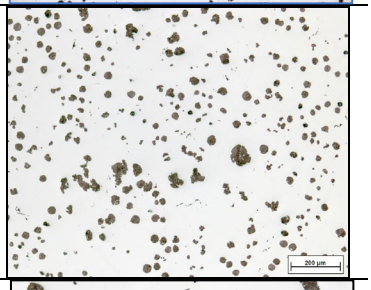
3.	Low Si	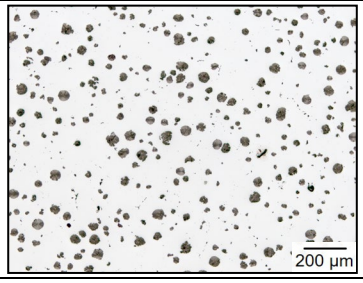	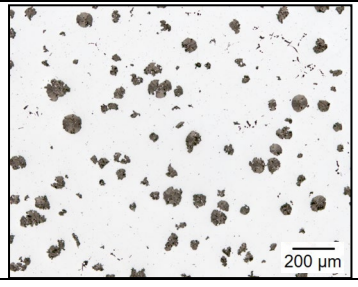	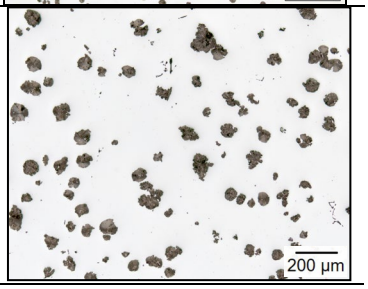

After software-assisted calculations, the results for these three values are presented in Figure 7-8-9. The findings for Nodularity and Nodule Count are entirely consistent with the previously shared expectations. Although there are some deviations in the Graphite Content ratios, these deviations are within acceptable tolerances.

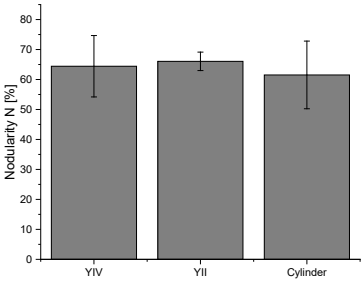

Fig. 7. Nodularity; medium Si content

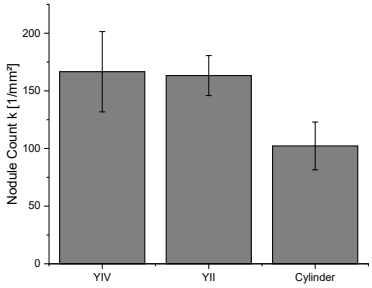

Fig. 8. Nodule count; medium Si content

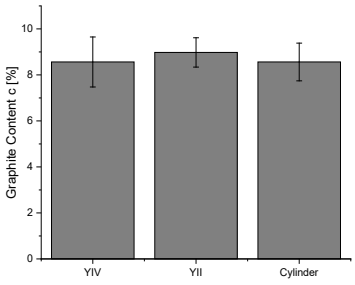

Fig. 9. Graphite content; medium Si content

3.2. Microstructure Results

At the beginning of the microstructural analysis of the remelted surface layers, the surface treated with a laser power of P_L=300 W and four repetitions n=4 was examined in cross sections by light microscopy. These parameters resulted in the largest remelting depth and the lowest surface roughness. The region referred to as the remelted layer is clearly visible in Figure 10. The remelted layer is free of cracks and graphite inclusions.

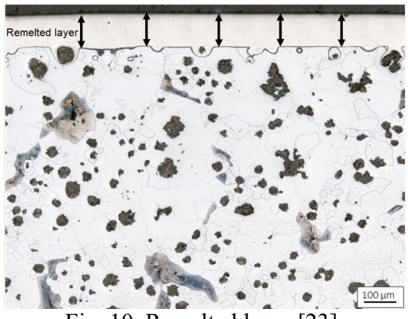

Fig. 10. Remelted layer [23]

In addition, scanning electron microscopy (SEM) and electron backscatter diffraction (EBSD) analysis of this region provided detailed information about the microstructure (Figure 11 a and b). Upon examination, distinct regions within the surface structure were identified. EBSD analysis confirmed that an austenitic structure formed in the upper region of the remelted layer. The EBSD results indicate the presence of body-centered cubic (bcc) and face-centered cubic (fcc) phases in the iron matrix. The red bcc phases represent ferrite, while the blue fcc phases correspond to austenite. Graphite particles were easily distinguishable in both the SEM and EBSD images. A ferritic structure was observed beneath the remelted layer, with a thin martensitic layer detected between the original ferritic structure and the newly formed austenitic surface layer. The remelted layer was largely free of graphite particles. [23]

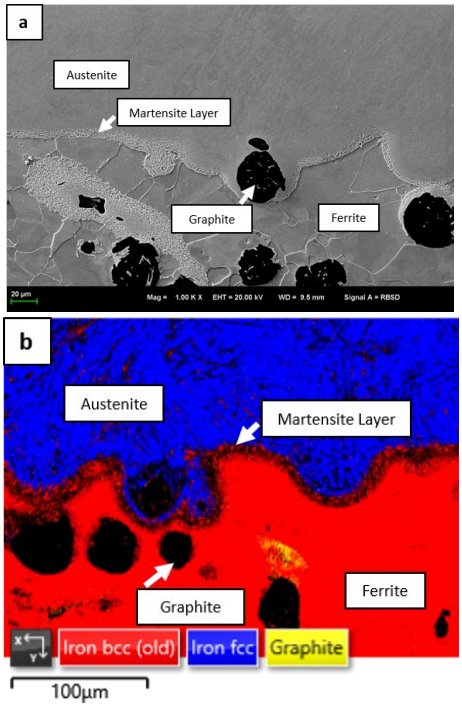

Fig. 11. a) SEM Image b) EBSD Image [23]

As stated in the "Experimental Method" section, to select the appropriate laser power (P_L) and number of repetitions (n), the most challenging conditions for these two parameters that can affect the surface quality, were determined first. To observe any cracks that might appear on the laser polished surface, the samples with the highest Si content were treated. First, two different levels of laser power P_L=200 W and P_L=300 W were applied. As expected, greater surface damage was observed at the higher laser power.

Additionally, samples with high silicon content exhibited graphite particles along the remelted depth in contrast to samples with lower silicon levels. This is expressed in the graphite structure circled in following figures. The number of repetitions was kept constant at n = 1 to isolate the effect of the laser power parameter.

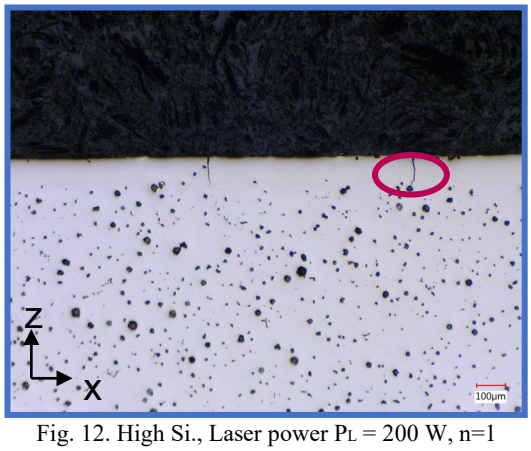

Fig. 12. High Si., Laser power P_L = 200 W, n=1

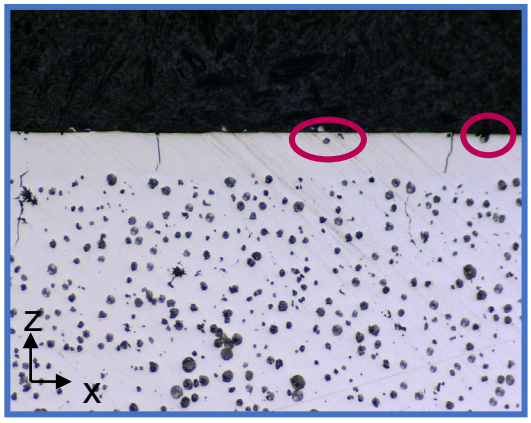

Fig. 13. High Si., Laser power P_L = 300 W, n=1

The first parameter, laser power, was set to P_L=300 W as this power level has a stronger impact on the surface and allows for processing future samples under worst-case scenario conditions (Figure 12-13).

In the next step, the number of repetitions was considered as the second parameter, with values of n = 1, n = 2, and n = 4 being applied respectively. The results indicated that the most significant crack damage in the surface structure occurred at n=4 (Figure 13-14-15). Thus, after examinations on the samples with the highest silicon content, it was determined that applying a laser power of P_L=300 W and and four repetitions (n = 4) would be appropriate for samples with other silicon levels.

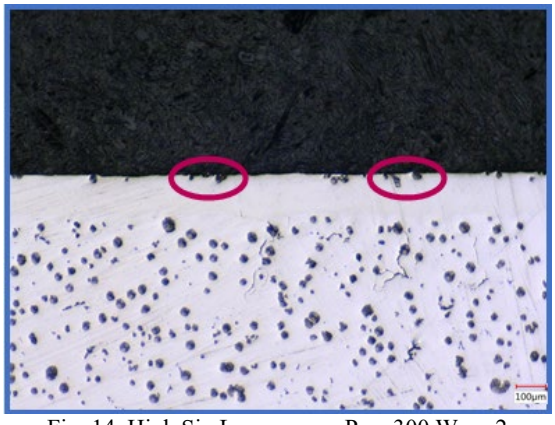
Fig. 14. High Si., Laser power P_L = 300 W, n=2

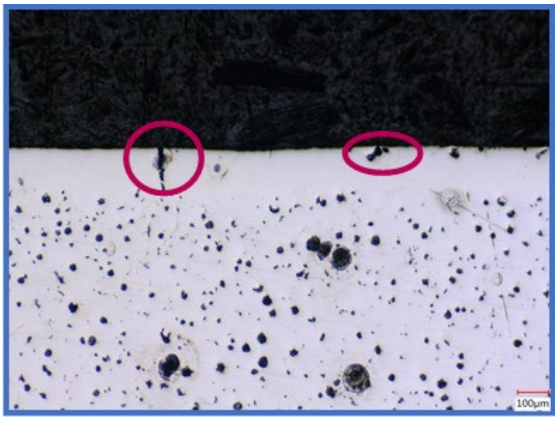
Fig. 15. High Si., Laser power P_L = 300 W, n=4

Finally, the laser power (P_L=300 W) and the number of repetitions (n=4) parameters, which were determined based on the examination of the high silicon content samples, were applied to the average silicon (Ave. Si) and low silicon (Low Si) samples. The chemical composition of these samples is detailed in Table 1. Upon examining the remelted zone of the other samples were examined, it was observed that no crack formation occurred. This shows that the silicon level is important and should be kept below a certain threshold in cast iron parts that are intended for laser polishing. (Figure 16-17).

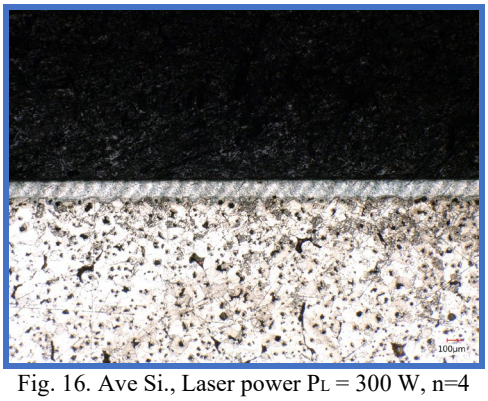
Fig. 16. Ave Si., Laser power P_L = 300 W, n=4

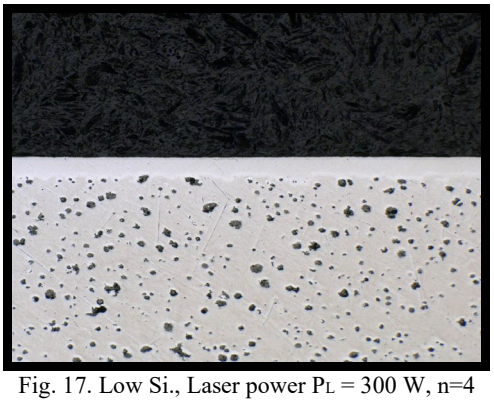

Fig. 17. Low Si., Laser power P_L = 300 W, n=4

4. Conclusion and Outlook

SGI alloys offer several advantages that make them viable alternatives to the hot-work steels currently used as molding materials, such as for glass. However, they also have some disadvantages, including low hardness and high surface roughness, which may limit their use. One method to reduce these disadvantages is laser polishing. However, laser polishing can cause surface defects depending on the chemical composition of the alloys. In this study, SGI alloys were cast in three different geometries and with three different silicon (Si) levels to assess this effect. The castings were then subjected to laser polishing using appropriate laser parameters, and the resulting microstructure was analyzed to understand the details post-laser application.

Different laser powers (200W - 300W) and numbers of laser passes (n=1, n=2, and n=4) were applied to samples with high Si content. The results indicated that a Si content of 4.25 wt% led to surface cracks, whereas no cracks were observed at Si levels of 3.52 wt% and 2.84 wt%. Consequently, lower Si levels (3.52 wt% and 2.84 wt%) are recommended to avoid surface cracking.

The novelty of this work is that it presents a viable alternative for laser polishing by examining different casting parameters in combination with different laser parameters.

The most important feature of this study, which distinguishes it from other studies, is to investigate the effect of the element Si, which is one of the chemical compositions thought to affect the laser polishing process applied to SGI Castings, whose use may be limited due to their mechanical properties and hardness values. This study will provide a new perspective to the researchers working on this subject by providing information on the appropriate Si level for laser polishing to improve mechanical and hardness properties.

In addition, this study offers a strong potential for future work to study the different elements in the chemical composition of this cast iron material in future studies. In this aspect, it not only shows the effect of the chemical composition of the cast iron material on laser polishing, but also opens up new topics for new studies in which the effects of different elements can be examined.

Acknowledgements

This research was funded by the Federal Ministry for Economic Affairs and Climate Action, grant number 22681. The authors would like to thank all project partners involved in this project and all colleagues at RWTH Aachen GI (*Gießerei Institut*) and Fraunhofer ILT (*Institut für Lasertechnik*).

References

[1] Prucha, T.E., Twarog, D., Monroe, R.W. (2008). *History and trends of metal casting*. ASM Handbook. https://doi.org/10.31399/asm.hb.v15.a0005186.

[2] Lopez, V., Bello, J.M., Ruiz, J. & Fernandez, B.J. (1994). Surface laser treatment of ductile irons. *Journal of Materials Science.* 29, 4216-4224 DOI:10.1007/bf00414201. https://doi.org/10.1007/BF00414201.

[3] Guo, X., Stefanescu, D.M., Chuzhoy, L., Pershing, M. A. & Biltgen, G.L. (1998). A mechanical properties model for ductile iron. *AFS Transactions*. 105, 47-54.

[4] Labrecque, C. & Gagné, M. (1998). Review ductile iron: fifty years of continuous development. *Canadian Metallurgical Quarterly.* 37(5), 343-378. https://doi.org/10.1179/cmq.1998.37.5.343.

[5] Alhussein, A., Risbet, M, Bastien, A., Chobaut, J.P., Balloy, D. & Favergeon, J. (2014). Influence of silicon and addition elements on the mechanical behavior of ferritic ductile cast iron. *Materials Science and Engineering: A*. 605, 222-228. DOI: 10.1016/j.msea.2014.03.057.

[6] Hatate, M., Shiota, T., Takahashi, N. & Shimizu, K., (2001). Influences of graphite shapes on wear characteristics of austempered cast iron. *Wear.* 251, (1-12), 885-889. https://doi.org/10.1016/S0043-1648(01)00746-3.

[7] Temmler, A., Willenborg, E., & Wissenbach, K. (2012). Laser polishing. In Laser Applications in Microelectronic and Optoelectronic Manufacturing (LAMOM) XVII, February 2012 (Vol. 8243, pp. 171-183). SPIE.

[8] Temmler, A., Cortina, M., Ross, I., Küpper, M.E. & Rittinghaus, S.K., (2022). Evolution of surface topography and microstructure in laser polishing of cold work steel 1.2379 (AISI D2) using quadratic, top-hat shaped intensity distributions. *Materials*. 15(3), 769, 1-27. https://doi.org/10.3390/ma15030769.

[9] Fernández-Vicente, A., Pellizzari, M. & Arias, J.L. (2012). Feasibility of laser surface treatment of pearlitic and bainitic ductile irons for hot rolls. *Journal of Materials Processing Technology*. 212(5), 989-1002. https://doi.org/10.1016/j.jmatprotec.2011.11.013.

[10] Catalán N., Ramos-Moore, E., Boccardo, A. & Celentano, D. (2022). Surface laser treatment of cast irons: a review. *Metals*. 12(4), 562, 1-28. https://doi.org/10.3390/met12040562.

[11] Grum, J. & S˘turm, R. (1996). Microstructure analysis of nodular iron 400-12 after laser surface melt hardening. *Materials Characterization.* 37(2-3), 81-88. https://doi.org/10.1016/S1044-5803(96)00063-0.

[12] Kiedrowski, T., & Wissenbach, K. (2004). Laser beam polishing of cast iron. *Fraunhofer ILT Annual Report*, 78.

[13] Ukar, E., Lamikiz, A., Liébana, F., Martinez, S., Tabernero, I. (2015). An industrial approach of laser polishing with differentlaser sources. *Materials Science & Engineering Technology.* 46, 661-667. https://doi.org/10.1002/mawe.201500324.

[14] Ukar, E., Lamikiz, A., Martinez, S. & Tabernero, I. (2014). Polishing of ductile cast iron with scan-head guided fiber laser. *Materials Science Forum.* 797, 151-156. https://doi.org/10.4028/www.scientific.net/MSF.797.151.

[15] Ukar, E., Lamikiz, A., Martínez, S., Estalayo, F. & Tabernero, I. (2013). Laser polishing of GGG70L cast iron with 2D scan-head. *Procedia Engineering.* 63, 53-59. https://doi.org/10.1016/j.proeng.2013.08.199.

[16] DIN EN 1563:2019-04; Founding—Spheroidal Graphite Cast Irons. Deutsches Institut fur Normung: Berlin, Germany, 2019.

[17] Benyounis, K.Y., Fakron, O., Abboud, J.H., Olabi, A.G. & Hashmi, M. (2005). Surface melting of nodular cast iron by Nd-YAG laser and TIG. *Journal of Materials Processing Technology*. 170(1-2), 127-132. https://doi.org/10.1016/j.jmatprotec.2005.04.108.
[18] Pagano, N., Angelini, V., Ceschini, L. & Campana, G. (2016). Laser remelting for enhancing tribological performances of a ductile iron. *Procedia CIRP*. 41, 987-991. DOI:10.1016/j.procir.2015.12.131.
[19] Nusser, C., Kumstel, J., Kiedrowski, T., Andrei Diatlov A. & Willenborg, E. (2015). Process- and material-induced surface structures during laser polishing. *Advanced Engineering Materials*. 17(3), 268-277. https://doi.org/10.1002/adem.201400426.
[20] Poprawe, R. (2011). *Tailored light 2-laser application technology.* Berlin, Germany: Springer.
[21] Krishnan, A. & Fang, F. (2019). Review on mechanism and process of surface polishing using lasers. *Frontiers of Mechanical Engineering*. 14(3), 299-319. https://doi.org/10.1007/s11465-019-0535-0.
[22] Temmler, A., Willenborg E. & Wissenbach, K. (2015). Design surfaces by laser remelting. *Material Science & Engineering Technology*. 12(A), 419-430. https://doi.org/10.1016/j.phpro.2011.03.053.
[23] Kreinest, L., Schussler, J., Özaydin, O., Kochuthundil Subhash, S., Willenborg, E. & Buhrig-Polaczek, A. (2024). Laser remelting of ductile cast iron to achieve a graphite-free surface layer for enabling a manual high-gloss finish. *Metals.* 14(3), 347, 1-14. https://doi.org/10.3390/met14030347.